Acta Oceanol. Sin., 2022, Vol. 41, No. 1, P. 21–29
https://doi.org/10.1007/s13131-021-1916-x
http://www.aosocean.com
E-mail: ocean2@hyxb.org.cn

Distribution of gamma-ray radionuclides in surface sediments of the Kongsfjorden, Arctic: Implications for sediment provenance

Sheng Zeng[1], Binbin Deng[2], Jinlong Wang[1]*, Juan Du[3], Jinzhou Du[1]

[1] State Key Laboratory of Estuarine and Coastal Research, East China Normal University, Shanghai 200241, China

[2] Monitoring Center of Aquatic Environment of Pearl River Basin, Guangzhou 510611, China

[3] Research Centre for Eco-Environmental Engineering, Dongguan University of Technology, Dongguan 523808, China

Received 19 April 2021; accepted 13 July 2021

Abstract

The Kongsfjorden is highly sensitive region to climate variability, however, the study of gamma-ray radionuclides in related areas is relatively scarce. In this study, the grain size, total organic carbon (TOC), $^{13}C_{org}$ isotopes, and specific activities of seven gamma nuclides were analysed in surface sediments of the Kongsfjorden in the Arctic during the summer of 2017. The specific activities of $^{210}Pb_{ex}$, ^{137}Cs, ^{238}U, ^{226}Ra, ^{228}Ra, ^{228}Th, and ^{40}K were 12–256 Bq/kg, 0–3.8 Bq/kg, 25–42 Bq/kg, 24–38 Bq/kg, 22–40 Bq/kg, 22–40 Bq/kg, and 354–738 Bq/kg, respectively, with average values of (121±94) Bq/kg, (2.0±1.2) Bq/kg, (34±6) Bq/kg, (32±4) Bq/kg, (32±6) Bq/kg, (33±6) Bq/kg, and (611±119) Bq/kg. This study observed a significant positive correlation (r=0.845, p<0.05) between TOC and $^{210}Pb_{ex}$, highlighting the strong influence of organic matter on the distribution of $^{210}Pb_{ex}$. The boundary scavenging of ^{210}Pb from the open sea contributed 27.5%–46.2% to the total $^{210}Pb_{ex}$ in the sediments of the outer Kongsfjorden. The grain size was an important factor affecting the activity distribution of several radionuclides (^{238}U, ^{228}Ra, ^{228}Th, ^{226}Ra, and ^{40}K). The specific activity of ^{137}Cs indicated the transport of terrestrial materials from the exposed area of the Kongsfjorden. The sediments in the Kongsfjorden were derived from various material contributions of glacial meltwater debris, glacial rivers, bare soil, atmospheric deposition, and marine sources. This study explains the source of the Kongsfjorden sediment and the distribution characteristics of radionuclides, and illustrateas the main factors affecting the distribution of radionuclides, which provides a reference for the behavior of polar radionuclides in future research.

Key words: Kongsfjorden, sediment, TOC, radionuclide, sediment source

Citation: Zeng Sheng, Deng Binbin, Wang Jinlong, Du Juan, Du Jinzhou. 2022. Distribution of gamma-ray radionuclides in surface sediments of the Kongsfjorden, Arctic: Implications for sediment provenance. Acta Oceanologica Sinica, 41(1): 21–29, doi: 10.1007/s13131-021-1916-x

1 Introduction

Radionuclides are commonly used tracers of material source, transport, and transformation in marine research (Huang et al., 2013; Lydersen et al., 2014; Lepage et al., 2016; Wang et al., 2016). The enrichment of radionuclides in ecosystems poses potential radiation risks to all levels of organisms. The investigation of radionuclides not only contributes to the assessment and control of radioactive risks in the environment, but also helps to better understand the particle transport process (Wang et al., 2017; Botwe et al., 2019).

The U/Th decay series and ^{40}K in sediments are the dominant sources of natural radioactivity. ^{226}Ra and ^{210}Pb are the daughter nuclides of ^{238}U; and ^{228}Th and ^{228}Ra are the daughter nuclides of ^{232}Th. Homologous nuclides form long-term equilibriums once they are in balance for long periods in the natural environment. However, nuclides and their daughters often deviate from equilibrium due to the geochemical differences between homologous nuclides. For example, ^{210}Pb and Th isotopes have high particle affinity and are easily scavenged from the seawater, whereas U and Ra have low particle affinity and mainly occur in seawater in their dissolved forms (Li et al., 1984; Chen et al., 2005). ^{238}U in seawater decays to ^{230}Th, which is scavenged from the water to the sediment by particulate matter and subsequently decays to ^{226}Ra. Therefore, ^{238}U is deficient relative to ^{226}Ra in modern deep-sea sediments, while $^{226}Ra/^{238}U$ verges on equilibrium in terrestrial minerals, and the deviation degree from equilibrium is generally smaller than that in deep-sea sediments. Hence, $^{226}Ra/^{238}U$ can be used to distinguish marine sediments from terrestrial sediments (Li et al., 1984; Huang et al., 2013; Mao et al., 2018). The ^{226}Ra in the sediment decays further to inert gas ^{222}Rn, of which segmental ^{222}Rn is emitted from the sediment to the atmosphere and decays to ^{210}Pb. ^{210}Pb adsorbs onto dust particles in aerosols and finally returns to the ground via dry or wet atmospheric deposition to form excess $^{210}Pb_{ex}$ (the additional input of ^{210}Pb to the sediment by atmospheric deposition, which differs from $^{210}Pb_{su}$ generated by *in situ* ^{222}Rn). Therefore, ^{210}Pb in modern sediments and shallow soil usually consists of both $^{210}Pb_{ex}$ and $^{210}Pb_{su}$ (Mabit et al., 2014). ^{137}Cs is an anthropogenic radionuclide that is mainly sourced from atmospheric thermonuclear weapon experiments and accident emissions from nuclear facilities, such as the Chernobyl disaster in 1986. In the coastal zone, terrigenous transportation is one of the main sources of ^{137}Cs (Lima et al., 2005).

The Kongsfjorden is an open glacier fjord located in the west

Foundation item: The National Natural Science Foundation of China under contract Nos 41706089 and 42107251.
*Corresponding author, E-mail: jlwang@sklec.ecnu.edu.cn

of Spitsbergen Island. A few studies have reported on the specific activity of gamma radionuclides in the soil of the Kongsfjorden area (Dowdall et al., 2003; Gwynn et al., 2004), but the research mainly focused on assessing modern sedimentation rates in the fjord using ^{210}Pb and ^{137}Cs (Aliani et al., 2004; Zaborska et al., 2006; Koziorowska et al., 2017). Abundant information on the interactions between fjord, land, and glacier environments have been recorded in fjord sediments, which provides an excellent basis for the study of the fjord environment in polar regions under the influence of climate change. Therefore, the gamma radionuclides in the surface sediments of the Kongsfjorden were studied, and provided some basic parameters for understanding the behaviour and transportation of natural radionuclides and ^{137}Cs in polar region. This study also discussed the source of the Kongsfjorden sediment and the main factors affecting the distribution of radionuclides. It is expected to provide new insight in understanding sediment dynamics in polar regions.

2 Materials and methods

2.1 *Study area*

The Kongsfjorden is 20 km long and 4–10 km wide, with a maximum depth of over 350 m (Glasser and Hambrey, 2001; Zaborska et al., 2006). Figure 1a shows the Western Spitsbergen Current (WSC), the Spitsbergen Trough Current (STC), and the Spitsbergen Polar Current (SPC) outside the Kongsfjorden (Husum et al., 2019). The WSC carries Atlantic water into the Kongsfjorden each summer, but less exchange between the fjord and outer sea occurs in winter (Berge et al., 2015; Koziorowska et al., 2017). Glaciers are a main factor affecting the environment in Kongsfjorden. During the meltwater season, substantial amounts of meltwater and glacial debris flow into the fjords through rivers (Zajaczkowsk, 2008; Lydersen et al., 2014). The inflow of lower-density freshwater to the fjords carries substantial amounts of suspended sediment to form meltwater plumes in the fjord surface water. The Bayelva River discharged 27×10^6 m^3/a to more than 40×10^6 m^3/a freshwater and 5 126 t/a to 22 797 t/a sediment between 1990 and 2001 (Bogen and Bønsnes, 2003). More recently, 29×10^6 m^3 freshwater and (6 400±1 300) t sediment flowed into the fjord area in 2012 (Zhu et al., 2016). Climate change significantly influences the water exchange between the fjord and the Atlantic, as well as the melting of terrestrial glaciers; therefore, fjords are highly sensitive regions to climate variability (Shi et al., 2018). Rivers formed by valley glaciers are important sources of freshwater and sediments to the fjords, which affects the distribution of nuclides in the sediments. Moreover, the Kongsfjorden is divided into the outer fjord in the west and the inner fjord in the east by the Blomstrandhalvøya boundary.

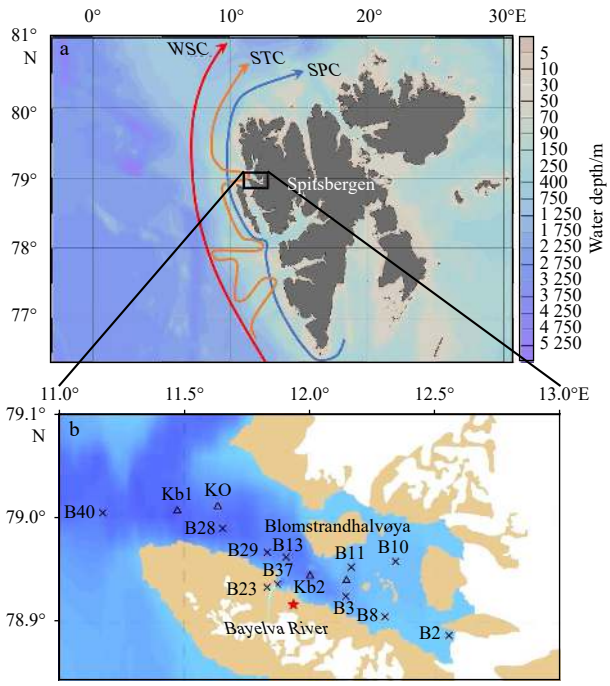

Fig. 1. Ocean current diagram modified from Husum et al. (2019) (a); study area and sampling locations (b). The Western Spitsbergen Current (WSC), the Spitsbergen Trough Current (STC), and the Spitsbergen Polar Current (SPC) outside the Kongsfjorden are shown in a. In b, black cross represents sampling sites of this study; hollow triangle, sampling sites from reference; red pentangle, Arctic Yellow River Station; white areas, glaciers; brown areas, unglaciated land; blue areas, marine.

2.2 *Sampling and analysis*

From August 22 to September 5, 2017, surface sediment samples were collected using a grab dredger and preserved in a self-sealing plastic bag. The specific sampling points are shown in Fig. 1b.

The grain size of the sediments was measured using a Malvern laser grain-size analyser MS-2000 (Malvern Instruments, UK; measuring range: 0.02–2 000 μm, repeated measurement error <3%). Approximately 0.1–0.2 g of dry sediment was mixed with 5 mL of 10% H_2O_2 and 5 mL 0.2 mol/L HCl to remove organic matter and metal oxides. After standing for 24 h, sodium hexametaphosphate solution (10 mL 0.5 mol/L) was added as the dispersant, followed by a water bath ultrasound for 10 min; the grain size of the sample was then measured on the laser analyser.

The total organic carbon (TOC) of the sediments was measured using an elemental analyser (Vario Macro CNS) with a standard deviation less than 0.1% and recovery more than 99.5%. The detection limit is 0.000 4 mg. The sediments were dried at 40°C and passed through an 80-mesh sieve, and approximately 1 g of the screened samples were weighed for further treatment. After soaking in 10% HCl, the sample was washed with ultra-pure water until neutral, and then dried again at 40°C. Approximately 0.03–0.04 g sample was then weighed and wrapped in tin foil for testing (Ma et al., 2020). The $^{13}C_{org}$ isotope ratio ($\delta^{13}C_{org}$) of the organic matter was determined using a Thermo isotope ratio mass spectrometer (DeltaPlusXP, Thermo Electron Corporation, Germany). Pee Dee Belemnite was used as the standard material with a determination accuracy of 0.2‰ (Zhu et al., 2020).

After drying the sediments using a freeze-dryer, 60 g sediments were sealed into a sample box (diameter 70 mm, height 70 mm), ground evenly, and stored for 21 d. ^{210}Pb, ^{226}Ra, ^{137}Cs, ^{40}K, ^{228}Th, ^{228}Ra, and ^{238}U radionuclides were measured using an ultra-low background HPGE gamma spectrometer (Canberra, USA; instrument energy measurement range: 10 keV–2 000 MeV; relative efficiency >35%; background value: ~0.9 counts per second (3 keV–2 GeV)). The shielding chamber of the instrument composed of 15 cm low-background lead, lined with 1 mm tin and 1.5 mm high-purity copper (Wu et al., 2011). To ensure the reliability of the QA/QC method, the efficiency calibration used the Laboratory Sourceless Calibration Software (LABSOC) and a standard sample (GBW04127). The measurement time was 12–24 h. The specific activity of radionuclides was calculated by the area of corresponding energy peaks on the energy spectrum; the corresponding energy peaks, branching ratios and detection limits

were 46.5 keV, 4.25%, 14.3 Bq/kg for ^{210}Pb; 661.6 keV, 85.1%, 0.83 Bq/kg for ^{137}Cs; 1 460.8 keV, 10.7%, 28.5 Bq/kg for ^{40}K; 351.9 keV, 37.6% and 609.3 keV, 37.6% (double peak), 3.0 Bq/kg for ^{226}Ra; 238.6 keV, 100% and 583.2 keV, 85.2% (double peak), 3.3 Bq/kg for ^{228}Th; 338.3 keV, 11.4% and 911.2 keV, 27.7% (double peak), 4.5 Bq/kg for ^{228}Ra; and 63.3 keV, 4.84%, 6.3 Bq/kg for ^{238}U. In the energy peaks corresponding to the above nuclides, ^{226}Ra, ^{228}Ra, and ^{238}U used the energy peaks of the daughter nuclides ^{214}Pb, ^{228}Ac, and ^{234}Th, respectively, and ^{228}Th used the daughter ^{212}Pb (238.6 keV, 100%) and ^{208}Tl (583.2 keV, 85.2%) (Du et al., 2010; Huang et al., 2013). The specific activity of $^{210}Pb_{ex}$ in the sample was determined by deducting the specific activity of ^{226}Ra from the total specific activity of ^{210}Pb. The specific activity of all short half-life nuclides was corrected by calibration back to the specific activity at the sampling time. The ^{238}U nuclides were measured after the sample was stored for six months to ensure a balance between ^{238}U and its daughter nuclides.

2.3 *Data calculation formula*

The formula for calculating the $^{210}Pb_{ex}$ inventory in the sedimentary column is as following (Appleby, 2004):

$$A = \int_{i=1}^{n} \rho \times (d_i - d_{i-1}) \times C_i, \quad (1)$$

where A is the $^{210}Pb_{ex}$ inventory (kBq/m^2); ρ is the sediment density (kg/m^3), i.e., the average sediment density (1 100 kg/m^3) of the adjacent stations; n is the depth of the $^{210}Pb_{ex}$ value close to zero; d_i is the depth of layer i (m); and C_i is the mass specific activity of sediments in layer i (Bq/kg).

The formula for calculating the contribution of the outer seawater to lead is as following:

$$C = \left(^{210}Pb_{ex}^{T} - {}^{210}Pb_{ex}^{I}\right) / {}^{210}Pb_{ex}^{T}, \quad (2)$$

where C is the contribution of the outer sea; $^{210}Pb_{ex}^{T}$ is the total inventory of $^{210}Pb_{ex}$ in the station; and $^{210}Pb_{ex}^{I}$ is the total inventory of $^{210}Pb_{ex}$ from terrestrial sources, the atmosphere, and the *in situ* decay of ^{226}Ra.

3 Results

3.1 *Distribution characteristics of surface sediment physical and chemical properties*

The grain size and TOC of the surface sediments are listed in Table 1. The mean grain size range of surface sediments from the Kongsfjorden was 4.9Φ–7.4Φ. The sand contents of the surface sediments at stations B2, B37, and B40 were 23.1%, 38.4%, and 16.2%, respectively, with averages of 5.8Φ, 4.9Φ, and 6.3Φ, respectively. For the remaining stations, the surface sediment sand content was ⩽5.4%, with smaller grain sizes ranging from 6.7Φ to 7.4Φ. These sediments were mainly composed of clay and silt, with clay and silt contents of 21.9%–29.9% and 67.9%–77.1%, respectively. Overall, except for B2, B37, and B40, the composition and average grain size of surface sediments at the remaining stations were similar. The TOC content in the study area ranged from 0.13% to 1.64%, showing an overall increasing trend from the inner to the outer fjord. The lowest TOC content was 0.13% at B2, and the highest TOC content was 1.64% at B40. In this study, the $\delta^{13}C_{org}$ ratio in the surface sediments of the Kongsfjorden ranged from –23.6% to –20.7%, and there were no obvious regional variability.

3.2 *Radionuclide distribution*

The specific activity of radionuclides in the surface sediments and surface soils of the Kongsfjorden are listed in Table 2. The specific activities of $^{210}Pb_{ex}$, ^{137}Cs, ^{238}U, ^{226}Ra, ^{228}Ra, ^{228}Th, and ^{40}K were 12–256 Bq/kg, 0–3.8 Bq/kg, 25–42 Bq/kg, 24–38 Bq/kg, 22–40 Bq/kg, 22–40 Bq/kg, and 354–738 Bq/kg, with average values of (121±94) Bq/kg, (2.0±1.2) Bq/kg, (34±6) Bq/kg, (32±4) Bq/kg, (32±6) Bq/kg, (33±6) Bq/kg, and (611±119) Bq/kg, respectively.

The distribution of ^{238}U, ^{228}Ra, ^{228}Th and ^{40}K specific activities were similar, showing an upward trend from the inner fjord to the outer fjord in the south of the fjord, but there were high values in B10 and B11, and low values in B40 (Figs 2a and c–e). The specific activity of ^{226}Ra was higher in the middle of the study area and lower at both ends, with a high value near the Blomstrandhalvøya (Fig. 2b). Overall, the specific activities of ^{238}U, ^{228}Th, ^{228}Ra, ^{226}Ra, and ^{40}K were higher in the sediments near the Blomstrandhalvøya, but lower in the outermost fjord and glacier front. The specific activity of ^{137}Cs first increased and then decreased from the inner to the outer fjord (Fig. 2g). The maximum ^{137}Cs value was observed at B13 near the Blomstrandhalvøya (3.8 Bq/kg), and the minimum value was below the detection limit at B2. The specific activity of $^{210}Pb_{ex}$ increased gradually from the inside to the outside of the inner fjord, but this study observed no obvious variation trend in the outer fjord (Fig. 2f). The specific activity of $^{210}Pb_{ex}$ in the outer fjord (189–256 Bq/kg) was much higher than that in the inner fjord (12–102 Bq/kg), with the highest values observed at B29 and B40, and the lowest value observed at B2 (Fig. 2f). One surface soil sample was collected at B23 near the Bayelva River. The specific activity of $^{210}Pb_{ex}$, ^{137}Cs, ^{238}U, ^{226}Ra, ^{228}Ra, ^{228}Th, and ^{40}K at this station were (32±4) Bq/kg, (9.8±0.5) Bq/kg, (30±4) Bq/kg, (27±1) Bq/kg, (30±2) Bq/kg, (28±1) Bq/kg, and (407±16) Bq/kg, respectively.

Table 1. Sediment characteristics

Station	Latitude	Longitude	Depth/m	Clay/%	Silt/%	Sand/%	Mean grain size	TOC/%	$\delta^{13}C$/‰
B2	78.872 2°N	12.578 2°E	65	15.6	61.3	23.1	5.8Φ	0.13	–20.7
B8	78.905 1°N	12.297 2°E	45	22.5	77.1	0.4	6.9Φ	0.21	–23.0
B10	78.958 2°N	12.340 0°E	62	29.9	70.1	0.0	7.4Φ	0.26	–22.5
B11	78.952 6°N	12.163 6°E	99	26.6	72.8	0.6	7.2Φ	0.51	–21.9
B3	78.924 4°N	12.142 6°E	117	21.9	74.6	3.6	6.7Φ	0.83	–22.5
B13	78.962 3°N	11.904 0°E	356	26.2	72.7	1.2	7.1Φ	0.77	–22.6
B37	78.936 3°N	11.870 2°E	5	12.8	48.9	38.4	4.9Φ	0.61	–23.6
B28	78.990 0°N	11.652 0°E	300	26.7	67.9	5.4	6.9Φ	1.15	–22.7
B29	78.966 7°N	11.829 2°E	333	26.3	72.1	1.6	7.1Φ	0.90	–22.4
B40	79.004 7°N	11.175 2°E	272	27.2	56.6	16.2	6.3Φ	1.64	–22.2

Table 2. Activities of radionuclides (Bq/kg) in surface sediments and soil sample

Station	^{238}U	^{226}Ra	^{228}Ra	^{228}Th	^{40}K	^{210}Pb$_{ex}$	^{137}Cs	^{226}Ra/^{238}U
B2	25±4	31±3	29±2	32±1	477±5	12±5	–	1.2±0.2
B8	33±3	33±1	33±2	33±1	578±9	30±4	1.1±0.2	1.0±0.1
B10	39±5	32±1	36±2	38±1	738±14	47±5	1.2±0.3	0.82±0.11
B11	38±3	35±1	36±3	37±2	677±13	102±7	2.6±0.3	0.93±0.11
B3	34±6	38±3	34±3	36±2	696±14	96±7	1.7±0.5	1.1±0.2
B13	34±3	32±1	32±1	32±1	631±9	189±6	3.8±0.3	0.94±0.08
B37	25±2	24±1	22±1	22±1	354±6	31±3	1.7±0.2	1.0±0.1
B28	42±4	33±1	40±2	40±1	695±15	203±9	3.1±0.5	0.79±0.07
B29	37±4	33±1	33±2	36±1	685±13	256±8	3.3±0.3	0.92±0.09
B40	31±2	28±1	23±1	27±1	577±8	246±5	1.7±0.2	0.92±0.07
Average value[a]	34±6	32±4	32±6	33±6	611±119	121±94	2.0±1.2	0.96±0.32
B23 soil sample (0–5 cm)	30±4	27±1	30±2	28±1	407±16	32±4[d]	9.8±0.5[d]	0.91±0.04
Soil and sediment[b] (n=17)	17–134	12–137	N/A	N/A	31–564	N/A	0.6–101	N/A
Soil and sediment[c] (n=10)	17–68	21–70	N/A	N/A	115–564	N/A	0.6–27	N/A

Note: a, The value obtained in this study; b, the values of surface soil and sediment sample referred to Dowdall et al. (2003); c, surface soil and sediment sample referred to Gwynn et al. (2004); d, surface sediment at 0–1 cm; N/A, not available; –, the specific activity of the nuclide is below the detection limit 0.9 Bq/kg.

4 Discussion

4.1 *Distribution characteristics of grain size, TOC, and $\delta^{13}C_{org}$*

In summer, icebergs calved from glaciers enter the sea and migrate from the eastern land of the fjord to the inner fjord under the influence of the southeast monsoon. Icebergs gradually melt and release particulate matter when encountering warmer seawater. Large-sized particles are deposited first, while small particles are transported further into the fjord (Svendsen et al., 2002). In contrast, the major coastal current of the Kongsfjorden travels from west to east, and wave activity exerts a dominant grain-size sorting effect, resulting in a decreasing grain size trend from near- to offshore (Bourriquen et al., 2018). Therefore, the sand content of the surface sediment in the inner fjord reduced from east to west to Station B13.

Overall, the frequency distribution curves of the surface sediments in the Kongsfjorden were unimodal and bimodal, both of which contained a fine-grain sediment body with a similar peak shape. Singh et al. (2018b) found that the Kongsfjorden sediments were sourced from glacial meltwater in the fjord, while sediments in the outer fjord were also sourced from the WSC particulate matter.

Based on Fig. 3, the frequency percentage of the mean grain size at B40, B28, and B29 within 0–2Φ showed a notable peak, and the peak height increased with increasing distance from Blomstrandhalvøya. This peak likely signifies ocean-derived particles, which may be influenced by the input of source materials from the outer sea, resulting in the larger average grain size in surface sediments of B40. In terrestrial weathering products transported by glacial meltwater, large grain-size substances are easier to deposit, while small grain-size substances are transported over further distances (Shi et al., 2011, 2018). As B2 is located at the front of the glacier, the surface sediments of B2 showed a larger average grain size than those of other inner fjord sediments. Due to the rapid velocity reduction of outflowing water from the glacier outlet, 90% of the outflowing sediment with larger grain sizes was deposited within 400 m of the ice front, and the remaining smaller grain-sized particles in the glacial meltwater were transported and deposited in the inner fjord (Singh et al., 2018a). Therefore, the peak grain size of B2 was larger than that of the sediments at other stations (except B37 station in the estuary area). Due to its location between the passages of the inner fjord and the outer fjord, the sediment at B37 was also affected by glacial meltwater, the WSC, and the Bayelva River. The flow velocity significantly reduces when the rivers reach the sea; this decreases the sediment-carrying capacity of the water current, resulting in the deposition of larger-sized particles in the estuaries (Yang et al., 2017). Moreover, wave action and tidal currents transport ocean-derived particulate matter to the estuary due to the separation effect. Therefore, the frequency curve at B37 was characterised by a wide range and multiple peaks, inferring complex sedimentary dynamics and sediment sources at B37.

From Fig. 2h, the TOC shows an obvious growth trend from the inner to the outer fjord. The TOC content increased more than ten times from 0.13% of the innermost Station B2 to 1.64% of the outermost Station B40. This is consistent with the viewpoint of Bourgeois (Bourgeois et al., 2016) that the main sources of organic matter in the Arctic fjords are ocean and sea ice algae. The distribution characteristics of TOC may be caused by the following four factors: (1) glacier calving in summer transports a large amount of suspended particulate matter to the inner fjord, which causes poor water transparency. The depth of the euphotic layer at the front of the glacier is only 0.3 m (Hop et al., 2002), leading to limited primary productivity. Even in high biomass seasons, the close association between the inner fjord and glaciers limits phytoplankton biomass (Piquet et al., 2014). (2) The sedimentation rate in the outer fjord is lower than that of the inner fjord (Singh et al., 2018b), which dilutes the organic matter in the inner fjord. (3) A large proportion of the eastern glacial meltwater enters the inner fjord from the seafloor or slightly above the seafloor. Freshwater tends to rise due to its lower density, resulting in turbulent mixing and TOC entrainment (Torsvik et al., 2019), which causes poor organic matter preservation in the surface sediments of the inner fjord. (4) Nutrients brought by the WSC can improve the biological productivity of the outer fjord (Hegseth and Tverberg, 2013; Piquet et al., 2014), which is supported by the high TOC concentration in sediments of the outer fjord.

The $\delta^{13}C_{org}$ is widely used to trace and identify the origin of sediment organic matter (SOM) and to evaluate the transformation and mixing of different sources in SOM (Xu et al., 2020). Previous reports recorded a $\delta^{13}C_{org}$ value of –23.8‰ to –19.3‰ in autochthonous organic matter of the Kongsfjorden (Bourgeois et al., 2016), –24.3‰ to –23.5‰ for the soil near Bayelva River,

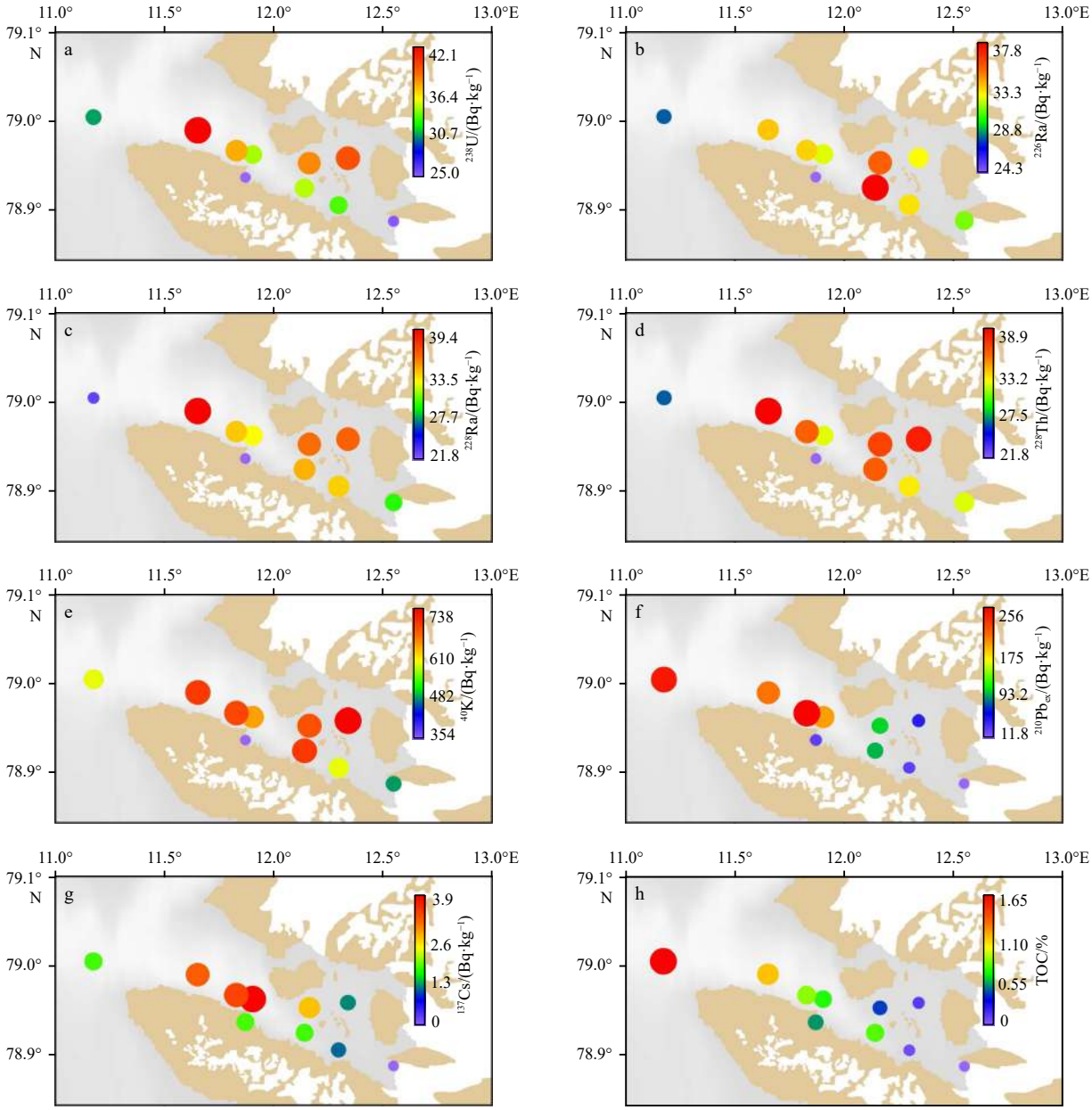

Fig. 2. Spatial distribution of radionuclides specific activity (Bq/kg) and TOC (%) in the surface sediments of the Kongsfjorden.

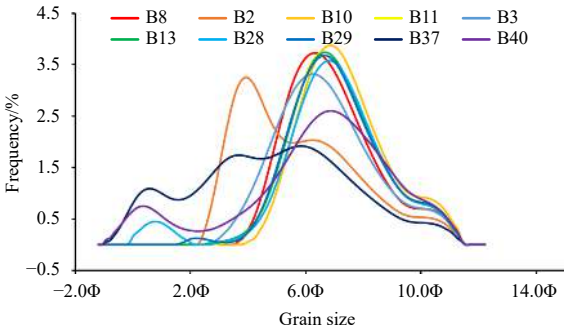

Fig. 3. Frequency percentage of mean grain size in surface sediment.

–26.1‰ to –22.8‰ for the Kongsfjorden surface water, and –25.2‰ to –23.8‰ for the Kongsfjorden bottom water (Zhu et al., 2016). B37 had the lowest $\delta^{13}C_{org}$ value of –23.6‰, which is in the range of the soil near the Bayelva River, autochthonous organic matter and sea surface water; this verifies the input of multiple material sources to B37, as concluded in the previous analysis. The $\delta^{13}C_{org}$ values of the other stations were mainly in the range of autochthonous organic matter, this suggests that most of the carbon in the surface sediments of the fjord was mainly derived from marine sources.

4.2 *Sediment cluster analysis*

Melting glaciers form rivers that transport large amounts of glacial debris to the fjords. These rivers also erode soil in the exposed area, resulting in two terrigenous signals in the terrigenous sediments of the Kongsfjorden: glacial debris and bare soil (Lizaga et al., 2019). In addition to surface runoff, the sediment sources in the Kongsfjorden include suspended dust from the atmosphere and particulate matter from outer seawater (Fig. 4).

In this study, the radionuclides, grain size, and TOC in the sediments were used to perform a cluster analysis on the physical properties of the sediments in the Kongsfjorden (Yang et al., 2017). According to Fig. 5, the physical properties of the sediments in the Kongsfjorden showed an axial clustering distribution; overall, the sediments can be divided into three categories related to the distance from the glacier in the east of the fjord: I, II and III. Category I comprises the glacier front and adjacent areas, Category II comprises the inner fjord away from the eastern glaciers, and Category III comprises the area outside the Blomstrandhalvøya. In this section, a simple analysis of the three sediment types was performed using the physical distance between different stations.

Category I sediments included Stations B2 and B8. As B2 and B8 are located on the main route of glacial meltwater into the sea, most of the sediments at these sites were derived from glacial solid materials (Zajaczkowsk, 2008). B3 is also located in the glacial meltwater path but is situated much further from the glacier front; therefore, the impact of glacial debris on B3 was less than that of *in situ* marine source materials from the inner fjord. B3 and B8 are both located in the southern land margin, but the sediment physical properties of B8 were more similar to that of B2 (at the glacier front) than B3 (Fig. 5). Therefore, compared with the effect of *in situ* marine source materials in the inner fjord, the impact of debris from the eastern fjord into the sea on Category I sediments was more significant. Category II sediments included Stations B11, B3, and B10. Restricted by the base between the inner and outer basins of the fjord (Svendsen et al., 2002), the inner fjord was less affected by the outer fjord and outer currents. The eastern glacier front is located far from the inner fjord; therefore, Category II sediments in the inner fjord are mainly affected by *in situ* marine sources. Category III sediments included Stations B40, B28, B29, and B13. Despite the presence of sediments from glacial meltwater, the outer fjord is mainly influenced by the inflow of materials and ice fragments from the Atlantic WSC (Svendsen et al., 2002; Hop et al., 2006), resulting in similar sediment compositions between the four stations in the outer fjord.

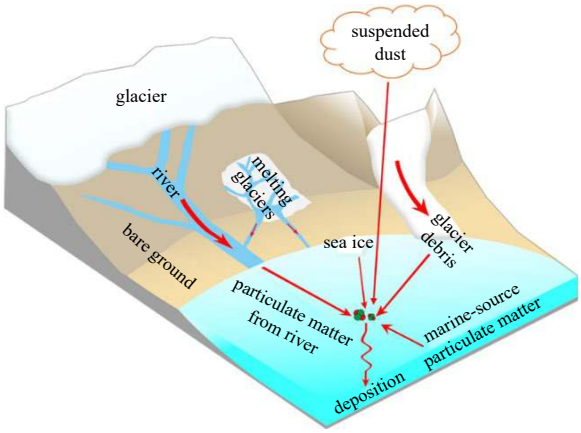

Fig. 4. Schematic diagram of the Kongsfjorden terrestrial sediment sources.

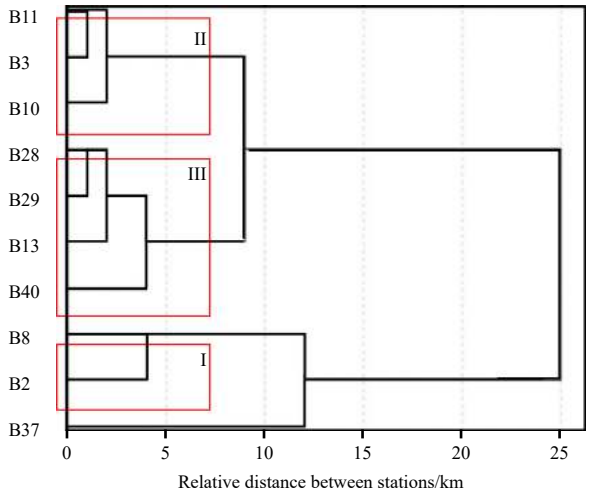

Fig. 5. Hierarchical clustering analysis shows the relevant associations among the locations (squared Euclidean distance, average linkage).

B37 is located downstream of a glacial river formed by valley glaciers. The site has similar material sources to that of Category I sediments, as both are influenced by glacial detritus. However, due to the combined action of rivers and seas in the process of glacial meltwater flux to the sea, the sediments accumulate both terrigenous materials from the Bayelva River and marine sources from the Kongsfjorden and the WSC; the sediment characteristics of the glacier are therefore different to those of Category I sediments. As shown in Fig. 5, the physical properties of the sediments at B37 are significantly different to those at nearby stations (i.e., B3, B11, and B13), indicating that the Bayelva River was less affected by surface sediments at stations outside the estuary area. This finding is consistent with the results of Wadham et al. (1998) and Zhu et al. (2016), which found that estuaries and glacier fronts are the main subsidence areas of materials carried by glacial meltwater.

4.3 *Correlation analysis between sediment characteristics and radionuclides*

According to Table 3, ^{238}U, ^{228}Ra, ^{228}Th, ^{226}Ra, and ^{40}K showed a good linear relationship with sediment grain size (r values are –0.793, –0.768, –0.817, –0.783, and –0.919, respectively; p<0.05), which supports the fact that finer grained particles carry more radionuclides (Shi et al., 2018). This study observed a weak linear relationship between these five nuclides and TOC in the sediments, which suggests that biological activities had little influence on their sediment distributions. Wang et al. (2017) proposed the use of sediment ^{226}Ra/^{238}U ratios as tracers for the source of sedimentary particles in marine environments, as the sediment ^{226}Ra/^{238}U ratio in different regions is significantly different, and the desorption of ^{226}Ra and ^{238}U in seawater is less than 10%. The ^{226}Ra/^{238}U measured in the soil samples at B23 was 0.91±0.04. According to the average ^{226}Ra and ^{238}U values reported by Dowdall et al. (2003) and Gwynn et al. (2004), the ^{226}Ra/^{238}U values of soil sample were 1.02 and 1.2, respectively, while the ^{226}Ra/^{238}U in the surface sediments of the Kongsfjorden was 0.79–1.2, which was similar to the soil values around the Kongsfjorden. This indicates that the surface sediments of the Kongsfjorden may be mostly terrestrially sourced.

In contrast to the previous five radionuclides, this study observed no clear linear relationship between the specific activity of ^{137}Cs and sediment grain size (r=–0.342), which suggests that sediment grain size had little influence on the spatial distribution of ^{137}Cs in sediments. ^{137}Cs is evenly distributed horizontally and vertically in the Kongsfjorden, and the specific activity of ^{137}Cs is similar to that of the outer seawater, showing a relatively conservative behaviour in the fjord (Gwynn et al., 2004). Wojtasik et al. (2017) found a strong exponential relationship between the con-

Table 3. Linear relationship between radionuclide activity, grain size, and TOC in surface sediments

	^{137}Cs	^{40}K	^{226}Ra	^{210}Pb$_{ex}$	^{238}U	^{228}Ra	^{228}Th	AGS	TOC
^{137}Cs	1.000								
^{40}K	0.412	1.000							
^{226}Ra	0.201	0.800*	1.000						
^{210}Pb$_{ex}$	0.745*	0.418	0.088	1.000					
^{238}U	0.548	0.911*	0.645*	0.426	1.000				
^{228}Ra	0.310	0.817*	0.830*	0.080	0.855*	1.000			
^{228}Th	0.234	0.885*	0.862*	0.143	0.852*	0.965*	1.000		
AGS	−0.342	−0.919*	−0.783*	−0.406	−0.793*	−0.768*	−0.817*	1.000	
TOC	0.503	0.162	−0.131	0.845*	0.181	−0.221	−0.153	−0.088	1.000

Note: *, significant correlation at 0.05; AGS, average grain size; TOC, total organic carbon.

centration of organic matter in the sediments of the Spitsbergen coast and ^{137}Cs (r^2 = 0.745 8). However, this study observed no exponential correlation between TOC and ^{137}Cs in this study (r^2 = 0.176 9). Among the clay minerals, ^{137}Cs has a higher affinity for illite than kaolinite and chlorite. Moreover, the desorption ratio of Cs to seawater was found to be <7% (Takata et al., 2015). As the clay minerals in the sediments of Kongsfjorden were mainly composed of illite (69%–78%) (Shi et al., 2018), the desorption of terrigenous ^{137}Cs particles in seawater is small, and ^{137}Cs is therefore well preserved in the surface sediments. ^{137}Cs in the marine source mainly exists in the water column in its dissolved form (Wang et al., 2017), and ^{137}Cs in the atmosphere cannot be deposited in soil covered by glaciers. Therefore, the specific activity of ^{137}Cs in the surface sediments reflects the signal of terrigenous material in unglaciated land of Spitsbergen. The highest ^{137}Cs value was observed in the soil sample at B23. Similarly, higher surface sediment ^{137}Cs values were observed in Stations B28, B29, and B13, indicating higher proportions of terrigenous substances from unglaciated land transported to these stations.

This study observed a significant linear relationship between the specific activity of ^{210}Pb$_{ex}$ and TOC (r=0.845, p<0.05), but the linear relationship between ^{210}Pb$_{ex}$ and sediment grain size was weak (r=–0.406, p=0.244). This study proposes three reasons for the increase in ^{210}Pb$_{ex}$ specific activity in surface sediments from the eastern part to the mouth of the inner fjord: (1) WSC-transported nutrients increased the biomass in the outer fjord, which increased the particulate matter and TOC concentrations and enhanced the removal of ^{210}Pb in the outer fjord (Liu et al., 2006; Wang et al., 2016). (2) As the land area covered by glaciers is unaffected by atmospheric ^{210}Pb, and the ^{210}Pb$_{ex}$ contained in glacial debris is low, the ^{210}Pb concentration in glacial rocks should be proportional to the exposure time (Łokas et al., 2019). The sedimentation rate decreases rapidly from the inner to the outer fjord (Aliani et al., 2004; Zaborska et al., 2006; Koziorowska et al., 2017), and higher sedimentation rates reduce the amount of ^{210}Pb$_{ex}$ absorbed onto sediments per unit mass, which reduces the specific activity of ^{210}Pb$_{ex}$ in the sediments in the inner fjord. (3) Due to the preferential deposition of larger particles in the transport process, small particles with a high specific activity of nuclides are transported over further distances, resulting in an increase in ^{210}Pb$_{ex}$ specific activity of surface sediments from the inner to the outer fjord.

To further understand the source of ^{210}Pb$_{ex}$ in the surface sediments of Kongsfjorden and the factors influencing its spatial distribution, this study calculated the inventory of ^{210}Pb$_{ex}$ in the sediments using the reported ^{210}Pb$_{ex}$ profile data in the sedimentary column.

Based on the study by Kuliński et al. (2014) and Koziorowska et al. (2017), the inventory of ^{210}Pb$_{ex}$ in the sedimentary column was calculated using Eq. (1). The ^{210}Pb$_{ex}$ of the cores KO, Kb1 and Kb2, has reached zero on the cores, so their inventory of ^{210}Pb$_{ex}$ can be calculated directly. KO is 17.8 kBq/m^2, Kb1 is 24.0 kBq/m^2, Kb2 is 12.9 kBq/m^2, and Kb1>KO>Kb2. The results show that the ^{210}Pb$_{ex}$ inventory in the outer fjord was much higher than the ^{210}Pb$_{ex}$ inventory in atmospheric deposition in the same latitudinal area (0.16–2.24 kBq/m^2) (Baskaran, 2011; Sanchez-Cabeza and Ruiz-Fernández, 2012); this suggests that the atmospheric fallout of ^{210}Pb was not the main source of sediment ^{210}Pb$_{ex}$ in the outer fjord. The average depths of the inner and outer fjord is 50 m (Elverhøi et al., 1980) and ~300 m (Bourgeois et al., 2016), respectively. According to the unreported data, the average specific activity of ^{226}Ra in the surface water of the fjord was (2.5±0.4) Bq/m^3. Considering the product of water depth and the specific activity as the inventory, the ^{226}Ra inventory in the inner fjord and outer fjord was 124 Bq/m^2 and 741 Bq/m^2, respectively. When comparing this to the sedimentary inventory of ^{210}Pb, this study can neglect the ^{210}Pb produced by the decay of ^{226}Ra in seawater.

It is assumed that the inventory of ^{210}Pb$_{ex}$ in the sediments of the Station Kb2 is equal to the total ^{210}Pb$^{I}_{ex}$ from terrestrial sources, the atmosphere, and the *in situ* decay of ^{226}Ra. According to Eq. (2), the offshore sea contributes 27.5%–46.2% of the total ^{210}Pb$_{ex}$ in the sediments of the outer fjord, indicating that the ^{210}Pb boundary scavenging is a main source of ^{210}Pb$_{ex}$ in the sediments of the outer fjord. This high contribution from the contribution of boundary scavenging to this study area is likely because the river discharge material is much smaller compared to other marginal sea, e.g., the East China Sea (Chung and Chang, 1995; Su and Huh, 2002).

5 Summary

This study analysed the horizontal distribution of particle size, TOC and its isotopes, and radionuclides in the surface sediments of Kongsfjorden, and deduced the following conclusions:

(1) Sediments from Category I stations consisted of larger particles derived from glacial debris, and sediments from Category II stations were composed of fine particles derived from glacial debris and *in situ* marine sources. Sediments from Category III sites were mainly derived from terrigenous sources with some contribution from marine sources, including *in situ* materials transported by the WSC. The material in the Bayelva estuary area was mainly composed of terrigenous coarse particles transported by glacial meltwater, while the remaining marine material was transported by wave and tidal action. The sediment grain size in the Kongsfjorden was mainly affected by the input of glacial debris and river and offshore material, and the main influen-

cing factors were regionally variable.

(2) The main sources of ^{238}U, ^{226}Ra, ^{228}Ra, ^{228}Th, ^{40}K, and ^{137}Cs were terrigenous soil. The spatial distributions of ^{238}U, ^{228}Ra, ^{228}Th, ^{226}Ra, and ^{40}K were closely related to the particle sizes of the sediments, as particles with finer diameters carry more radionuclides.

(3) This study observed no significant correlation between the five nuclides and TOC in the sediments, which suggests that the spatial distribution of the nuclides was less affected by biological activities. This study identified no significant correlation between ^{137}Cs, grain size, and TOC. The distribution of ^{137}Cs was affected by the state of land glacier coverage, and the high specific activity of ^{137}Cs in surface sediments reflects the terrigenous material signal of the unglaciated land in the Kongsfjorden.

(4) This study observed a good linear correlation between TOC and $^{210}Pb_{ex}$ in the surface sediments of the Kongsfjorden (r=0.845, p<0.01), indicating that TOC is an important factor affecting $^{210}Pb_{ex}$ distribution. Based on the inventory calculation, this study concluded that the boundary clearance of outer seawater contributes 27.5%–46.2% of the total $^{210}Pb_{ex}$ in outer fjord sediments, indicating that $^{210}Pb_{ex}$ in the outer fjord is mainly affected by sea-sourced materials, with lower contributions from terrestrial material and atmospheric deposition.

Acknowledgements

We thank two anonymous reviewers for their constructive comments for improvement of the original manuscript. We thank Zhuoyi Zhu for his assistance with field sampling.

References

Aliani S, Bartholini G, Degl'innocenti F, et al. 2004. Multidisciplinary investigations in the marine environment of the inner Kongsfiord, Svalbard islands (September 2000 and 2001). Chemistry and Ecology, 20(S1): S19–S28

Appleby P G. 2004. Environmental change and atmospheric contamination on svalbard: sediment chronology. Journal of Paleolimnology, 31(4): 433–443, doi: 10.1023/B:JOPL.0000022545.73163.ed

Baskaran M. 2011. Po-210 and Pb-210 as atmospheric tracers and global atmospheric Pb-210 fallout: a review. Journal of Environmental Radioactivity, 102(5): 500–513, doi: 10.1016/j.jenvrad.2010.10.007

Berge J, Heggland K, Lønne O J, et al. 2015. First records of Atlantic mackerel (*Scomber scombrus*) from the Svalbard archipelago, Norway, with possible explanations for the extension of its distribution. Archives, 68(1): 54–61

Bogen J, Bønsnes T E. 2003. Erosion and sediment transport in high Arctic rivers, Svalbard. Polar Research, 22(2): 175–189, doi: 10.3402/polar.v22i2.6454

Botwe B O, Schirone A, Delbono I, et al. 2019. Radioactivity concentrations and their radiological significance in sediments of the Tema Harbour (Greater Accra, Ghana). Journal of Radiation Research and Applied Sciences, 10(1): 63–71

Bourgeois S, Kerhervé P, Calleja M L, et al. 2016. Glacier inputs influence organic matter composition and prokaryotic distribution in a high Arctic fjord (Kongsfjorden, Svalbard). Journal of Marine Systems, 164: 112–127, doi: 10.1016/j.jmarsys.2016.08.009

Bourriquen M, Mercier D, Baltzer A, et al. 2018. Paraglacial coasts responses to glacier retreat and associated shifts in river floodplains over decadal timescales (1966–2016), Kongsfjorden, Svalbard. Land Degradation & Development, 29(11): 4173–4185

Chen Jinfang, Liu Guangshan, Huang Yipu. 2005. Disequilibrium of natural decay series in sediments of intertidal mudflats of Xiamen. Journal of Oceanography in Taiwan Strait, 24(3): 274–282

Chung Y, Chang W C. 1995. Pb-210 fluxes and sedimentation rates on the lower continental slope between Taiwan and the South Okinawa Trough. Continental Shelf Research, 15(2–3): 149–164, doi: 10.1016/0278-4343(94)E0023-F

Dowdall M, Gerland S, Lind B. 2003. Gamma-emitting natural and anthropogenic radionuclides in the terrestrial environment of Kongsfjord, Svalbard. Science of the Total Environment, 305(1–3): 229–240, doi: 10.1016/S0048-9697(02)00478-3

Du Jinzhou, Wu Yunfeng, Huang Dekun, et al. 2010. Use of ^{7}Be, ^{210}Pb and ^{137}Cs tracers to the transport of surface sediments of the Changjiang Estuary, China. Journal of Marine Systems, 82(4): 286–294, doi: 10.1016/j.jmarsys.2010.06.003

Elverhøi A, Liestøl O, Nagy J. 1980. Glacial erosion, sedimentation and microfauna in the inner part of Kongsfjorden, Spitsbergen. Norsk Polarinstitutt Skrifter, 172: 33–58

Glasser N F, Hambrey M J. 2001. Tidewater glacier beds: insights from iceberg debris in Kongsfjorden, Svalbard. Journal of Glaciology, 47(157): 295–302, doi: 10.3189/172756501781832331

Gwynn J P, Dowdall M, Davids C, et al. 2004. The radiological environment of svalbard. Polar Research, 23(2): 167–180, doi: 10.1111/j.1751-8369.2004.tb00006.x

Hegseth E N, Tverberg V. 2013. Effect of Atlantic water inflow on timing of the phytoplankton spring bloom in a high Arctic fjord (Kongsfjorden, Svalbard). Journal of Marine Systems, 113–114: 94–105

Hop H, Falk-Petersen S, Svendsen H, et al. 2006. Physical and biological characteristics of the pelagic system across Fram Strait to Kongsfjorden. Progress in Oceanography, 71(2–4): 182–231, doi: 10.1016/j.pocean.2006.09.007

Hop H, Pearson T, Hegseth E N, et al. 2002. The marine ecosystem of Kongsfjorden, Svalbard. Polar Research, 21(1): 167–208, doi: 10.3402/polar.v21i1.6480

Huang Dekun, Du Jinzhou, Deng Bing, et al. 2013. Distribution patterns of particle-reactive radionuclides in sediments off eastern Hainan Island, China: implications for source and transport pathways. Continental Shelf Research, 57: 10–17, doi: 10.1016/j.csr.2012.04.019

Husum K, Howe J A, Baltzer A, et al. 2019. The marine sedimentary environments of Kongsfjorden, Svalbard: an archive of polar environmental change. Polar Research, 38: 3880

Koziorowska K, Kuliński K, Pempkowiak J. 2017. Distribution and origin of inorganic and organic carbon in the sediments of Kongsfjorden, Northwest Spitsbergen, European Arctic. Continental Shelf Research, 150: 27–35, doi: 10.1016/j.csr.2017.08.023

Kuliński K, Kędra M, Legeżyńska J, et al. 2014. Particulate organic matter sinks and sources in high Arctic fjord. Journal of Marine Systems, 139: 27–37, doi: 10.1016/j.jmarsys.2014.04.018

Lepage H, Laceby J P, Bonté P, et al. 2016. Investigating the source of radiocesium contaminated sediment in two Fukushima coastal catchments with sediment tracing techniques. Anthropocene, 13: 57–68, doi: 10.1016/j.ancene.2016.01.004

Li Peiquan, Liu Zhihe, Lu Guangshan, et al. 1984. The geochemical studies of U, Th, Ra, K(^{40}K) in sediments of Okinawa Trough. Oceanologia et Limnologia Sinica, 15(5): 457–467

Lima A L, Bergquist B A, Boyle E A, et al. 2005. High-resolution historical records from Pettaquamscutt River basin sediments: 2. Pb isotopes reveal a potential new stratigraphic marker. Geochimica et Cosmochimica Acta, 69(7): 1813–1824, doi: 10.1016/j.gca.2004.10.008

Liu J P, Li A C, Xu K H, et al. 2006. Sedimentary features of the Yangtze River-derived along-shelf clinoform deposit in the East China Sea. Continental Shelf Research, 26(17–18): 2141–2156, doi: 10.1016/j.csr.2006.07.013

Lizaga I, Gaspar L, Quijano L, et al. 2019. NDVI, ^{137}Cs and nutrients for tracking soil and vegetation development on glacial landforms in the Lake Parón Catchment (Cordillera Blanca, Perú). Science of the Total Environment, 651: 250–260, doi: 10.1016/j.scitotenv.2018.09.075

Łokas E, Zaborska A, Sobota I, et al. 2019. Airborne radionuclides and heavy metals in high Arctic terrestrial environment as the indicators of sources and transfers of contamination. The Cryosphere, 13(7): 2075–2086, doi: 10.5194/tc-13-2075-2019

Lydersen C, Assmy P, Falk-Petersen S, et al. 2014. The importance of tidewater glaciers for marine mammals and seabirds in Sval-

bard, Norway. Journal of Marine Systems, 129: 452–471, doi: 10.1016/j.jmarsys.2013.09.006

Ma Fuwei, Li Maotian, Liu Yan, et al. 2020. Changes of nutrient salts deposited in the Burullus lagoon, Egypt: effects of human activity over the past century. Acta Sedimentologica Sinica, 38(6): 1249–1257

Mabit L, Benmansour M, Abril J M, et al. 2014. Fallout ^{210}Pb as a soil and sediment tracer in catchment sediment budget investigations: a review. Earth-Science Reviews, 138: 335–351, doi: 10.1016/j.earscirev.2014.06.007

Mao Yuanyi, Lin Jing, Huang Dekun, et al. 2018. Radionuclides in the surface sediments along the coast of Bailong Peninsula in Beibu Gulf. Journal of Applied Oceanography, 37(2): 194–202

Piquet A M T, van de Poll W H, Visser R J W, et al. 2014. Springtime phytoplankton dynamics in Arctic Krossfjorden and Kongsfjorden (Spitsbergen) as a function of glacier proximity. Biogeosciences, 11(8): 2263–2279, doi: 10.5194/bg-11-2263-2014

Sanchez-Cabeza J A, Ruiz-Fernández A C. 2012. ^{210}Pb sediment radiochronology: an integrated formulation and classification of dating models. Geochimica et Cosmochimica Acta, 82: 183–200, doi: 10.1016/j.gca.2010.12.024

Shi Fengdeng, Cheng Zhenbo, Wu Yonghua, et al. 2011. The research on glacial-marine deposit types and sedimentary processes in the Arctic Kongsfjorden. Haiyang Xuebao (in Chinese), 33(2): 115–123

Shi Fengdeng, Shi Xuefa, Su Xin, et al. 2018. Clay minerals in Arctic Kongsfjorden surface sediments and their implications on provenance and paleoenvironmental change. Acta Oceanologica Sinica, 37(5): 29–38, doi: 10.1007/s13131-018-1220-6

Singh N, Rajan S, Choudhary S, et al. 2018a. Diisopropylnaphthalene in the surface sediments of an Arctic fjord: environmental significance. Polar Science, 18: 142–146, doi: 10.1016/j.polar.2018.04.009

Singh N, Sivaramakrishnan R, Choudhary S, et al. 2018b. Spatial distribution and environmental assessment of heavy metals in the surface sediments of Kongsfjorden, Svalbard. Czech Polar Reports, 8(1): 1–23, doi: 10.5817/CPR2018-1-1

Su C C, Huh C A. 2002. ^{210}Pb, ^{137}Cs and ^{239,240}Pu in East China Sea sediments: sources, pathways and budgets of sediments and radionuclides. Marine Geology, 183(1–4): 163–178, doi: 10.1016/S0025-3227(02)00165-2

Svendsen H, Beszczynska-Møller A, Hagen J O, et al. 2002. The physical environment of Kongsfjorden-Krossfjorden, an Arctic fjord system in Svalbard. Polar Research, 21(1): 133–166

Takata H, Hasegawa K, Oikawa S, et al. 2015. Remobilization of radiocesium on riverine particles in seawater: the contribution of desorption to the export flux to the marine environment. Marine Chemistry, 176: 51–63, doi: 10.1016/j.marchem.2015.07.004

Torsvik T, Albretsen J, Sundfjord A, et al. 2019. Impact of tidewater glacier retreat on the fjord system: modeling present and future circulation in Kongsfjorden, Svalbard. Estuarine, Coastal and Shelf Science, 220: 152–165

Wadham J L, Hodson A J, Tranter M, et al. 1998. The hydrochemistry of meltwaters draining a polythermal-based, high Arctic glacier, south Svalbard: I. The ablation season. Hydrological Processes, 12(12): 1825–1849, doi: 10.1002/(SICI)1099-1085(19981015)12:12<1825::AID-HYP669>3.0.CO;2-R

Wang Jinlong, Du Jinzhou, Baskaran M, et al. 2016. Mobile mud dynamics in the East China Sea elucidated using ^{210}Pb, ^{137}Cs, ^{7}Be, and ^{234}Th as tracers. Journal of Geophysical Research, 121(1): 224–239

Wang Jinlong, Du Jinzhou, Bi Qianqian. 2017. Natural radioactivity assessment of surface sediments in the Yangtze Estuary. Marine Pollution Bulletin, 114(1): 602–608, doi: 10.1016/j.marpolbul.2016.09.040

Wojtasik B, Świrydowicz S, Burska D, et al. 2017. Radionuclide activities in sediments on the northern coast of Spitsbergen. Polish Polar Research, 38(3): 291–312, doi: 10.1515/popore-2017-0019

Wu Meigui, Du Jinzhou, Zhang Jing, et al. 2011. Seasonal properties and environmental signification of $^{210}Pb_{ex}$、$^{228}Th_{ex}$、^{7}Be and ^{137}Cs in surface sediment of tidal flat, Chongming, China. Marine Environmental Science, 30(6): 792–797

Xu Cheng, Yang Bin, Dan S F, et al. 2020. Spatiotemporal variations of biogenic elements and sources of sedimentary organic matter in the largest oyster mariculture bay (Maowei Sea), Southwest China. Science of the Total Environment, 730: 139056, doi: 10.1016/j.scitotenv.2020.139056

Yang Hui, Zheng Binxing, Yu Dongsheng, et al. 2017. Characteristics of surface sediment grain size and the erosion/deposition evolution in the outer Pinghai Bay, Fujian. Journal of Applied Oceanography, 36(2): 233–242

Zaborska A, Pempkowiak J, Papucci C. 2006. Some sediment characteristics and sedimentation rates in an Arctic Fjord (Kongsfjorden, Svalbard). Annual Environmental Protection, 8: 79–97

Zajaczkowsk M. 2008. Sediment supply and fluxes in glacial and outwash fjords, Kongsfjorden and Adventfjorden, Svalbard. Polish Polar Research, 29(1): 59–72

Zhu Zhuoyi, Wu Ying, Liu Sumei, et al. 2016. Organic carbon flux and particulate organic matter composition in Arctic valley glaciers: Examples from the Bayelva River and adjacent Kongsfjorden. Biogeosciences, 13(4): 975–987, doi: 10.5194/bg-13-975-2016

Zhu Kun, Wu Ying, Qi Lijun. 2020. Spatiotemporal variations and influencing factors of organic carbon content in the urban rivers of Shanghai. Journal of East China Normal University: Natural Science, (1): 150–158